J Appl Electrochem (2008) 38:1707–1714
DOI 10.1007/s10800-008-9620-5

ORIGINAL PAPER

Electrodeposition of NiCu-matrix nanocomposites using a rotating cylinder Hull cell

A. Lozano-Morales · E. J. Podlaha

Received: 26 February 2008 / Accepted: 2 June 2008 / Published online: 27 June 2008

Abstract The electrodeposition of NiCu composites using nanometric diameter alumina and ceria was examined using a rotating cylinder electrode (RCE) and a rotating cylinder Hull Cell (RCHC). The RCE polarization behavior was altered by the presence of particles (12.5 g L^{-1}) in the electrolyte. The RCHC was used to survey the composition and deposit thickness, and hence partial current densities in order to determine the cause for the polarization changes. It is the first use of the RCHC to evaluate composite electrodeposition. Cu reduction was inhibited with both alumina and ceria particles, but the nickel and side reaction rates were dependent on the particle type. Alumina particles imparted an enhancement affect on Ni and the side reaction, while ceria did the opposite, resulting in an inhibiting effect. The deposits contained more alumina than ceria, and the alloy composition was altered most with alumina present in the electrolyte compared to a particle-free electrolyte.

Keywords Electrodeposition · NiCu-alumina composites · NiCu-ceria composites

1 Introduction

The electrodeposition of alloy [1, 2] and metal matrix composite [3–6] materials has been of particular interest due to the unique and often superior properties compared to their constituent components. Combining them, fabricating metal composites composed of an alloy matrix, can provide additional flexibility in tailoring the deposit properties. Some examples of electrodeposited composites containing an alloy matrix include α-Al_2O_3 particles with a Cr–Ni alloy [7], α-Al_2O_3, and TiO_2 in NiCu [8] and our prior work with γ-Al_2O_3 in NiCu alloys [9, 10]. The interest in NiCu alloy materials are well known for their corrosion resistance [2, 11–15], thermoelectrical [16, 17], catalytic [18–20], and mechanical [8, 21, 22] properties. The electrodeposition of alumina particles in metal-matrix composites has also been widely studied [5, 6] because alumina improves not only mechanical properties [4, 23], but also thermal and mechanical stability at elevated temperatures [24].

There are few works related to the electrodeposition of NiCu matrix-composites and the influence of the particle on the metal matrix reduction rate and hence composition. Fawzy et al. [8] found that during the electrodeposition of NiCu alloys with α-Al_2O_3 and TiO_2, there was a shift in the total current density to more noble potentials and the resulting alloy composite had an expected increase in the microhardness compared to the alloy without particles. The depolarizing affect was greater the smaller the particle size. Lozano-Morales et al. [9, 25] also reported a similar enhancement in the Cu kinetic reduction rate with nanometer size alumina particles. Panda and Podlaha [10] studied the NiCu-γ-Al_2O_3 system for use in fabricating micro-patterned structures. In micro-recesses, the inclusion of alumina nanoparticles in solution, even in small quantities, helped to enhance mass-transport rates of Cu. Such an increase in the Cu limiting current density was also reported by Stojak and Talbot [26] in thin film deposition with high particle loadings. In this work the effect of

A. Lozano-Morales
Gordon and Mary Cain Department of Chemical Engineering, Louisiana State University, Baton Rouge, LA 70803, USA

E. J. Podlaha (✉)
Department of Chemical Engineering, Northeastern University, Boston, MA 02115, USA
e-mail: e.podlaha-murphy@neu.edu

nanometer size alumina and ceria particles on the copper and nickel deposition is studied with copper under diffusion control and the nickel kinetically controlled. Ceria inclusion into a metal matrix may have useful properties for corrosion protection. For example, a composite of CeO_2 particles dispersed in a chromium film demonstrated improved oxidation resistance [27]. Here, a comparison of the NiCu electrodeposition with ceria and alumina particles are examined using a rotating cylinder Hull cell (RCHC).

The RCHC is a tool that can be used to readily assess the variation in composition and thickness of a deposit over a wide range of applied current density [28–31]. The seminal work of Madore and Landolt [28] presented design conditions for obtaining a large variation in current distribution along the length of a cathode for the NiCu system. They demonstrated the deconvolution of partial current densities in a NiCu alloy by mapping the current distribution to a polarization curve. The work presented here will follow a similar approach, but to a composite system. It represents the first demonstration of the use of the RCHC to composite electrodeposition.

2 Experimental

Citrate electrolytes were composed of 0.025 M $CuSO_4$, 0.7 M $NiSO_4$, and 0.25 M $Na_3C_6H_5O_7$ with and without particles, at a pH of 4.5. Two types of particles were examined: γ-Al_2O_3 having an average diameter of 32 nm, supplied by Nanophase Technologies Corporation, IL, USA, and CeO_2, with a reported diameter size of 9–15 nm, supplied by Alfa Aesar, MA, USA. A low particle loading of 12.5 g L^{-1} was used so as not to significantly influence the hydrodynamics of the rotating cylinder electrode.

Two types of rotating cylinder electrode configurations were used, one with the conventional, nearly uniform, current distribution (RCE) and the other with a forced current distribution (RCHC) along the electrode length. The RCHC system (RotaHull, Eco Chemie B.V., RHC70006) included a rotating 410 stainless steel cylindrical rod working electrode with a 0.6 cm diameter and 8 cm length, and the anode was a platinum mesh. All the deposits were obtained using an average current density of -13 mA cm^{-2} for a period of 29 min. A computer controlled potentiostat and impedance system (Zahner IM6e) were used to measure polarization curves and ohmic resistance. Polarization curves were measured with and without particles on a rotating cylinder electrode (RCE) with variable rotation rates in the turbulent flow regime. A saturated calomel electrode was used as the reference electrode. All polarization scans were performed by increasing the cell potential from the open circuit value at a scan rate of 2 mV s^{-1} and corrected for ohmic drop with impedance spectroscopy. The agitation of the suspension was controlled by the rotating electrode hydrodynamics.

A Kevex Omicron energy dispersive X-ray fluorescence analyzer (XRF) was used to analyze the thickness and composition of the deposits. The XRF error is less than 0.5 wt% propagated to the calculation in current density. The ceria amount in the deposit was consistently below 1 wt%, and thus, its composition was confirmed using wavelength-dispersive X-ray spectroscopy (WDS) with a scanning electron microscope (SEM, JEOL JXA-733), which provides an order of magnitude higher precision. Thirty points were analyzed along each of the cylindrical cathodes. The partial current densities of Cu and Ni were obtained from the composition and thickness analysis using Faraday's law.

3 Results and discussion

A comparison of polarization curves obtained from the NiCu particle free electrolyte, and from the electrolytes containing particle loadings of 12.5 g L^{-1} alumina and ceria, is shown in Fig. 1, at a RCE working electrode having a rotation rate of 540 rpm. When ceria particles are present in the electrolyte the total current density is inhibited throughout the whole potential range. However, when alumina particles are present, the total current density is not affected until the potential is more negative than -0.7 V, where it is enhanced. In order to determine which reaction causes the change in the total current density, the partial current densities were inspected with the RCHC, with a forced variation of total current density along the electrode length.

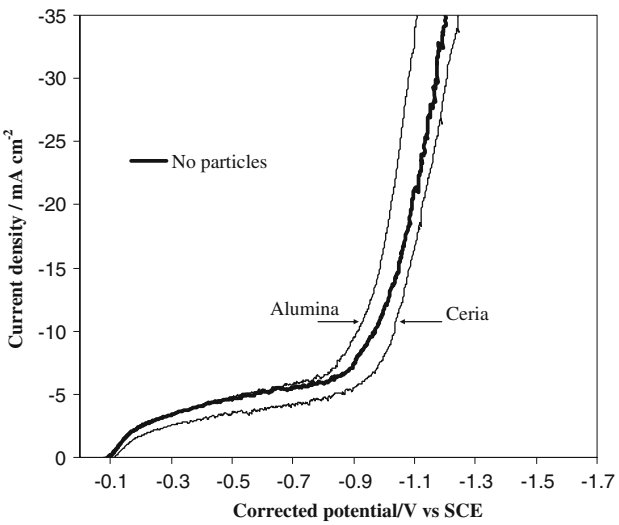

Fig. 1 RCE Polarization curves from the electrodeposition of a NiCu alloy for a particle free electrolyte and in the presence of alumina and ceria particles at 540 rpm

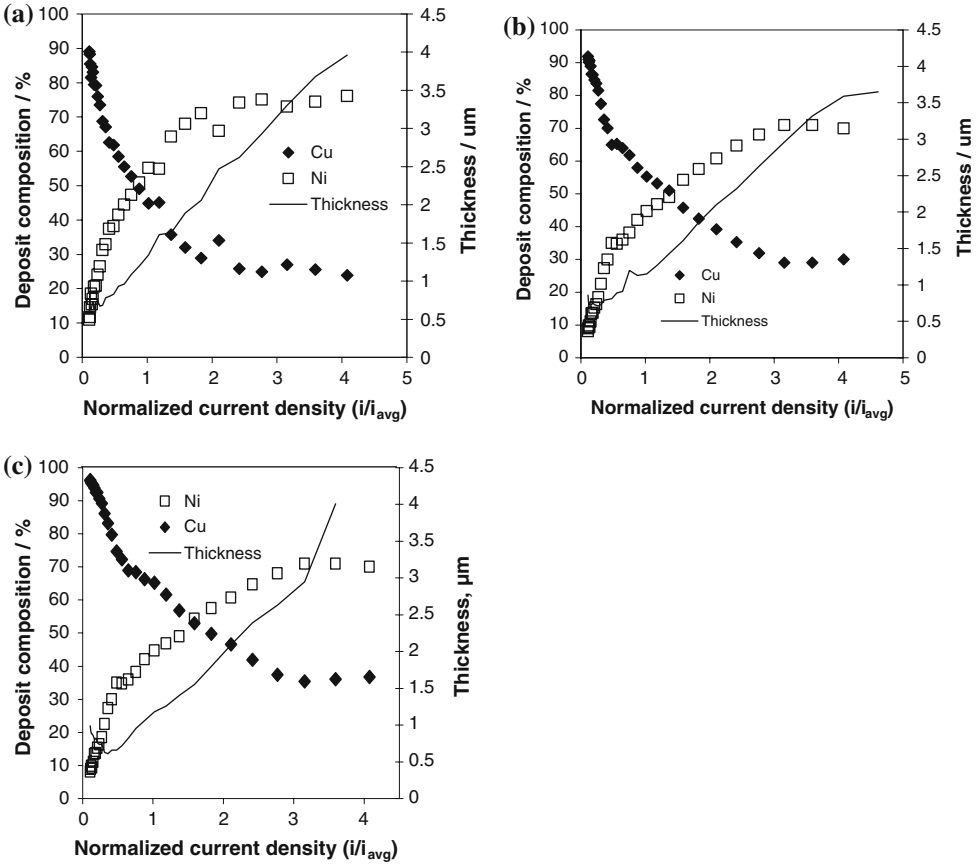

Fig. 2 Variation in thickness and composition for a NiCu alloy with normalized applied current density obtained from a particle free electrolyte at (**a**) 200, (**b**) 365 and (**c**) 540 rpm

A primary current distribution approach was taken to interpret the RCHC data (Appendix A) because it closely represents the current change along the electrode length and it can be modeled in an easy and tractable mathematical way. In order to evaluate the validity of using such an approach, the Wagner number, $Wa = \left(\frac{\kappa \partial E/\partial i}{L}\right)$, is required to be low ($\ll 1$) for the average current density employed in the RCHC. A low *Wa* indicates a large current distribution which then results in changes in deposit composition and thickness. Under these conditions, the RCHC operates as a tool for surveying electrodeposition conditions. In contrast a large *Wa* ($\gg 1$) indicates a dominate kinetic control and under these conditions the geometry of the cell would have little to no influence on the current distribution. Consequently for the RCHC, there would be no current distribution, and hence no composition or thickness variation. The conductivity, κ, measured for the electrolyte with no particles was 0.04 S cm^{-1}. From the polarization curve (Fig. 1) a slope $\partial E/\partial i$ of 22 mV cm^2 mA^{-1} was measured in the region where both copper and nickel deposit at the applied, average current density. The corresponding *Wa* for an electrode length, *L*, of 8 cm, under these conditions is 0.1. Therefore, the total current density distribution along the cathode of the RCHC configuration is governed largely by an ohmic control characteristic of primary current distribution. Another indirect check of a primary current distribution environment is due to the variation in composition that was observed along the electrode length presented in Figs. 2–4.

Figures 2–4 show the variation in thickness and alloy composition without (Fig. 2) and with alumina (Fig. 3) and ceria particles (Fig. 4) at different electrode rotation rates: (a) 200, (b) 365, and (c) 540 rpm on the RCHC. The particle concentrations are shown in Figs. 3d and 4d, respectively, for alumina and ceria. The measurements were taken at different positions along the electrode surface and the distance correlated to a normalized current density (Appendix A), expressed in the abscissa of the plots. The alloy thickness increased with current density but did not change significantly with rotation rate for all electrolytes.

The Cu composition of the resulting deposit was slightly affected by rotation rate, as expected, due to the transport control of the copper reduction reaction. Cu composition varied along the electrode length, and hence varied with current density, from 89 to 25, 92 to 29, and 96 to 35 wt.% for rotation rates of 200, 365, and 540 rpm, respectively, when no particles were present. The addition of particles lowered the Cu composition in the composite compared to the deposits without particles in the electrolyte. The copper

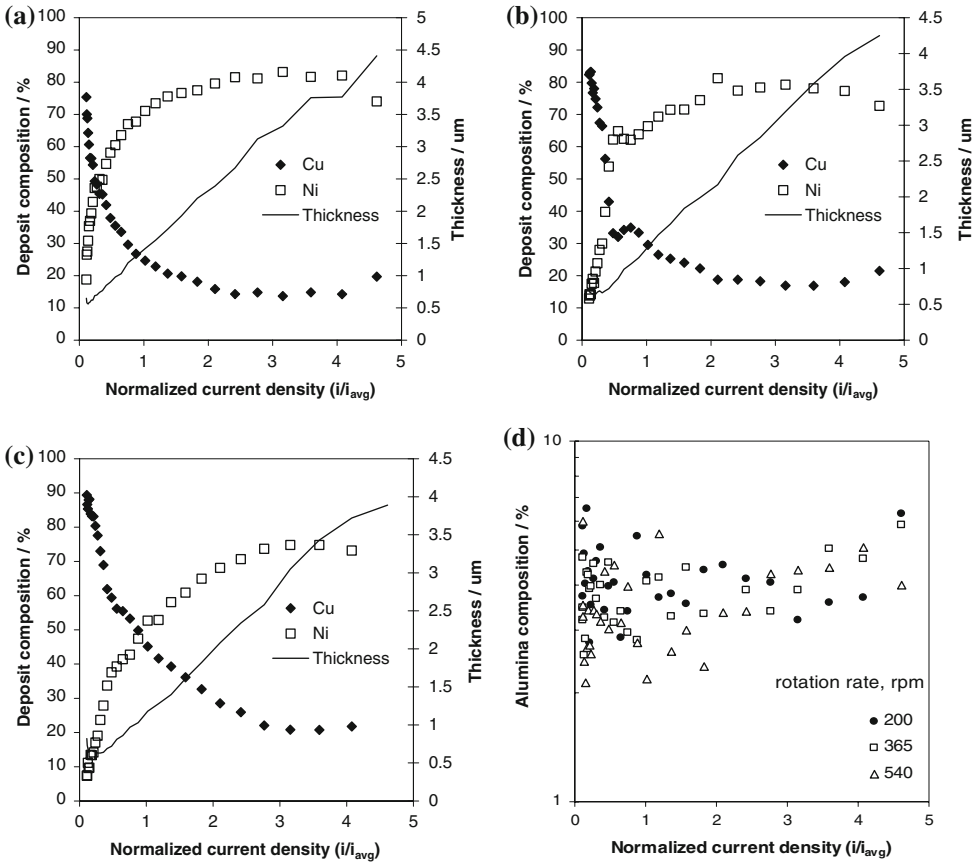

Fig. 3 Variation in thickness and Ni, Cu composition for the NiCu–Al_2O_3 composite with normalized applied current density at (**a**) 200, (**b**) 365, (**c**) 540 rpm; and (**d**) Al_2O_3 content for all rotation rates

composition variation when alumina particles were present, was 75–13, 83–16, and 90–20 wt.% for the three rotation rates investigated. The copper composition was lowered most significantly in the high current density range with both alumina and ceria. For example, at 540 rpm there is up to a 46% decrease of Cu in the material deposited from the alumina containing electrolyte and up to a 38% decrease of Cu in the ceria containing electrolyte compared to the NiCu alloy electrolyte without particles.

The alloy and composite thickness remained nearly the same for deposits from the particle free electrolyte and the particle containing electrolytes at 540 rpm. At lower rotation rate, when ceria particles were present, there was a slightly lowered deposit thickness near the high current density end, but at the low current density end there was a small increase in the thickness compared to the deposits without particles.

The minimum and maximum amounts of alumina in the deposits were (2.8, 6.5), (2.6, 5.9), and (2.2, 6.0) wt.% at 200, 365, and 540 rpm, respectively. The amount of ceria in the deposits were very low and fluctuated between 0.01 and 2.6 wt.% with current density for all rotation rates. Particularly for the ceria composite case, the change of the copper composition is not accounted for by the increase in mass by the particle, but must be due to the change in the copper and/or nickel reaction rates. Thus, the partial current densities were examined in order to further understand the interacting affect of the particle inclusion on the metal rates.

First, knowing the deposit composition and thickness, the corresponding partial current densities were calculated along the length of the cylinder cathode, then using the primary current distribution approach the total current density was determined as a function of the cathode length. The steady-state current-potential behavior is determined from polarization curves (Fig. 1) so that the partial current densities can be expressed on a potential scale.

The effect of different particles on the copper partial current density using a 12.5 g L^{-1} particle loading of alumina and ceria at an electrode rotation rate of 540 rpm is shown in Fig. 5. The copper partial current density remains constant over the entire potential range. The copper partial current density is inhibited when particles (either Al_2O_3 or CeO_2) are present in the electrolyte as shown in Fig. 5. The copper partial current density is less inhibited when ceria particles are present in the electrolyte. Since the copper partial current density is relatively flat, mass transport control of the copper reaction was examined by varying the rotation rate. The value of the copper current density at −0.5 V was determined at different rotation rates with and without the presence of particles in the electrolyte using the RCHC. According to the empirical expression by Eisenberg et al. [32] the limiting current density follows

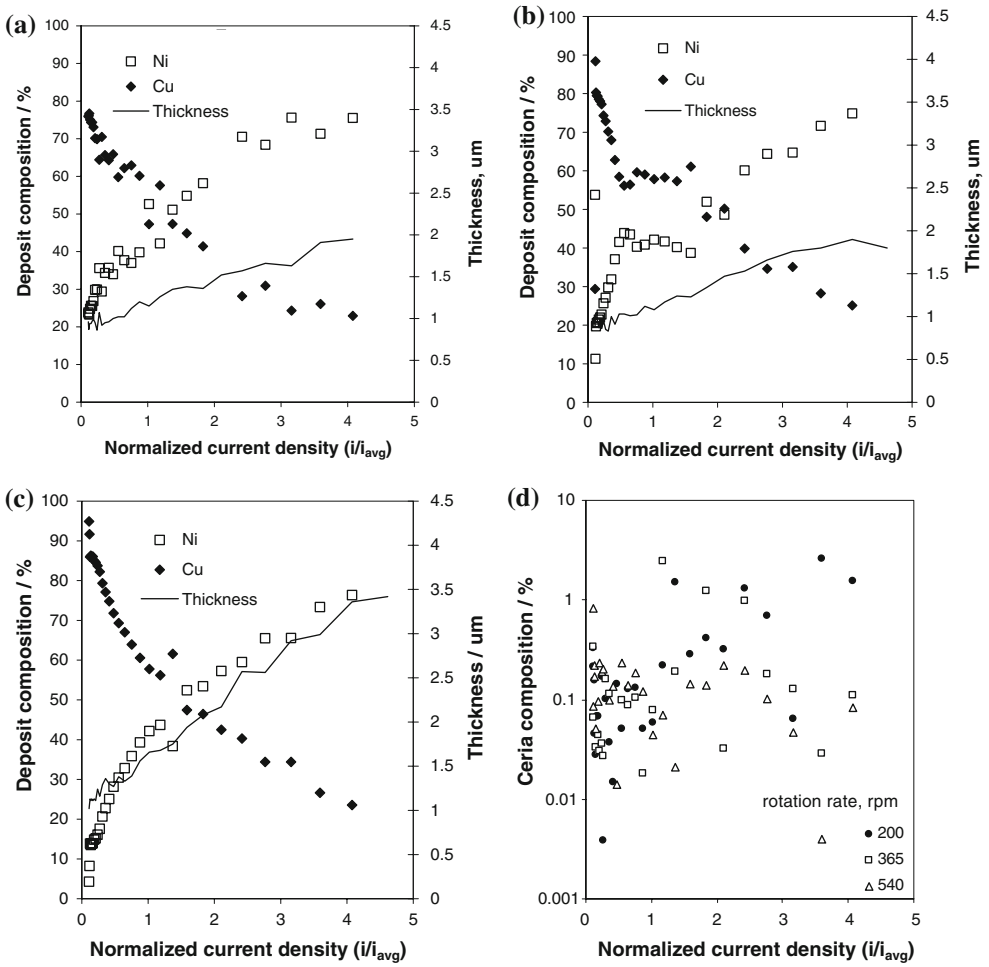

Fig. 4 Variation in thickness and Ni, Cu composition for a NiCu–CeO_2 alloy with normalized applied current density at (**a**) 200, (**b**) 365 and (**c**) 540 rpm; and (**d**) CeO_2 content for all rotation rates

$$i_L = 0.01nFC^b D^{0.644} v^{-0.344} S^{0.7} d_i^{0.4}$$

where n is the number of electrons transferred, F is Faraday's constant, C^b is the copper bulk concentration, D is the copper diffusion coefficient, v is the kinematic viscosity, S is the rotation speed (in rpm) and d_i is the cathode diameter. The diffusion coefficient of copper from the particle-free electrolyte was determined from the slope of a plot of the reciprocal of the limiting current density vs. the electrode rotation rate to the -0.7 power, (Fig. 5b), and found to be 1.1×10^{-6} cm^2 s^{-1} in agreement to the value reported by Madore and Landolt [28] for a similar citrate electrolyte. In the presence of particles, the copper partial current density did not change significantly with rotation rate and therefore is not indicative of a mass transport-limited behavior. Thus, at -0.5 V the copper rate with codepositing particles is still under kinetic control.

The nickel partial current density increases with potential in the kinetically-controlled region in all cases at an electrode rotation rate of 540 rpm (Fig. 6). In this case, the partial current density of nickel is also inhibited when ceria particles are present in the electrolyte, but there is a clear enhancement with the presence of alumina particles as shown. Table 1 lists the values of the nickel charge transfer coefficients from electrolytes with and without the presence of particles at 540 rpm, which were calculated from the slopes of Tafel plots as shown in the insert of Fig. 6. The Tafel slopes were calculated from high potentials (e.g. from -0.9 to -1.3 V) where nickel primary current distribution dominates. In the absence of particles in the electrolyte, a nickel charge transfer coefficient, α_{Ni}, was found to be equal to 0.21, similar to the value reported by Hessami and Tobias [33]. The presence of alumina particles in the electrolyte did not have a large effect on the nickel charge transfer value of 0.25, but with the presence of ceria particles in the electrolyte the nickel charge transfer coefficient decreased to 0.15.

The variation of the side reaction and current efficiency with potential during the electrodeposition of NiCu alloys

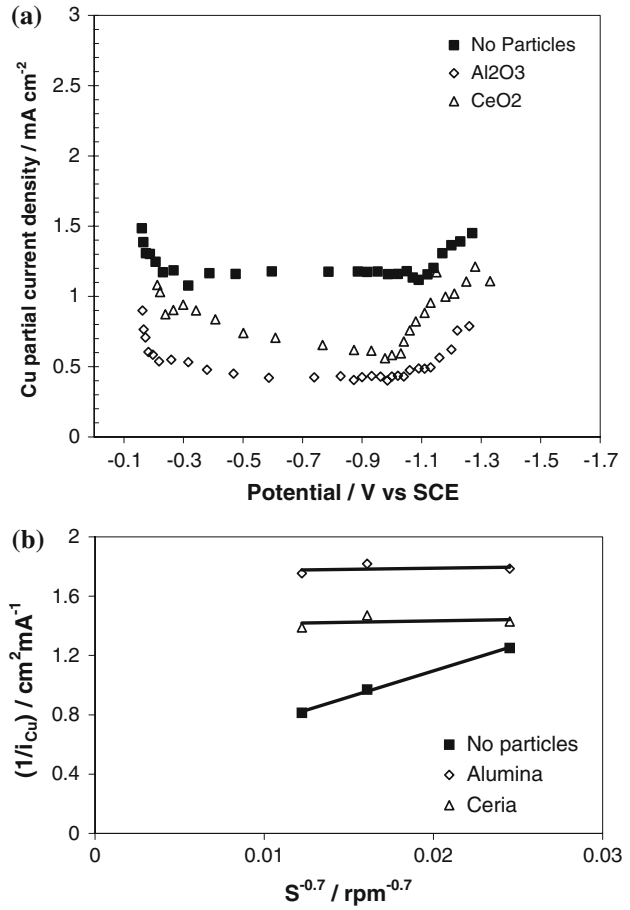

Fig. 5 Effect of different particles on the copper limiting current density along the potential region at (**a**) an electrode rotation rate of 540 rpm and (**b**) variable rotation rates at −0.5 V

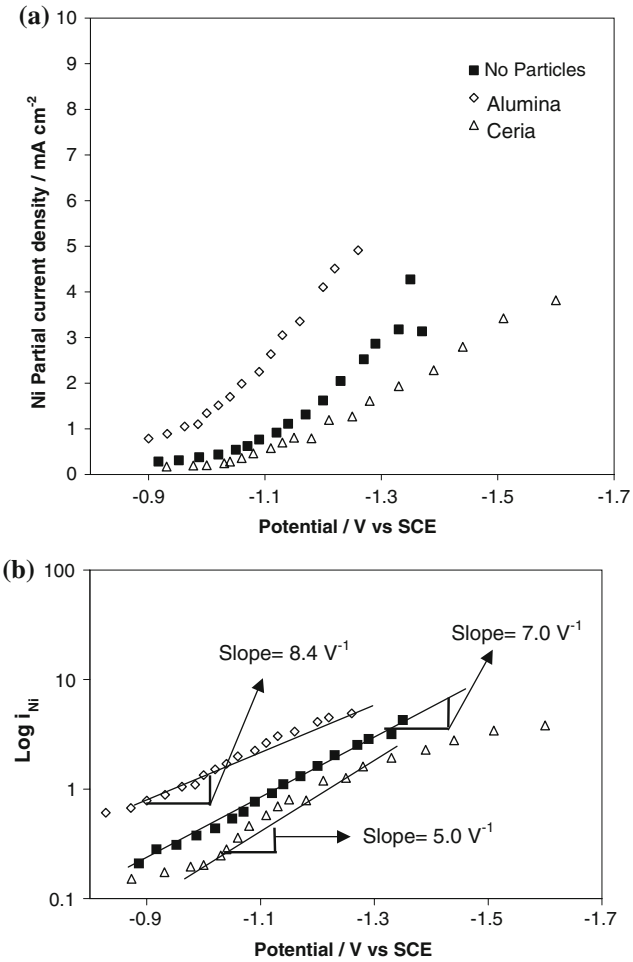

Fig. 6 Effect of different particles on the (**a**) nickel partial current density along the potential region at an electrode rotation rate of 540 rpm, and (**b**) linear regression on a semi-log plot

and NiCu-particle composites at 540 rpm is shown in Figs. 7a, b. In Fig. 7a the side reaction remains almost constant with potential in the region where copper deposition occurs, but at higher potentials (e.g. >−0.7 V) it increases exponentially, as expected for water reduction. The side reactions are highest when alumina particles are present in the electrolyte, and lowest with ceria. The corresponding current efficiencies for the electrodeposition of NiCu alloys and NiCu-particle composites are shown in Fig. 7b. In all cases the current efficiency decreases exponentially with potential. There is little change in current efficiency with the presence of particles, despite a change in the side reaction, because of the associated change in the metal partial current densities.

Table 1 Nickel charge-transfer coefficients with and without particles

	Inverse tafel slope (V^{-1})	α_{Ni}
No particles	16.1	0.21
Alumina	19.3	0.25
Ceria	11.5	0.15

4 Conclusions

Total polarization curves of NiCu-alumina and ceria composites deviated from the particle free electrolyte result. Hence, the partial current densities were examined using a RCHC. Particles did alter the alloy deposition rates even though their inclusion into the alloy was low. Ceria particles in the electrolyte resulted in a more sluggish copper, nickel, and water reduction kinetic behavior compared to a particle free, NiCu electrolyte. The copper current density was decreased with the addition of alumina particles in the electrolyte, but the nickel and side reaction deposition rate was enhanced.

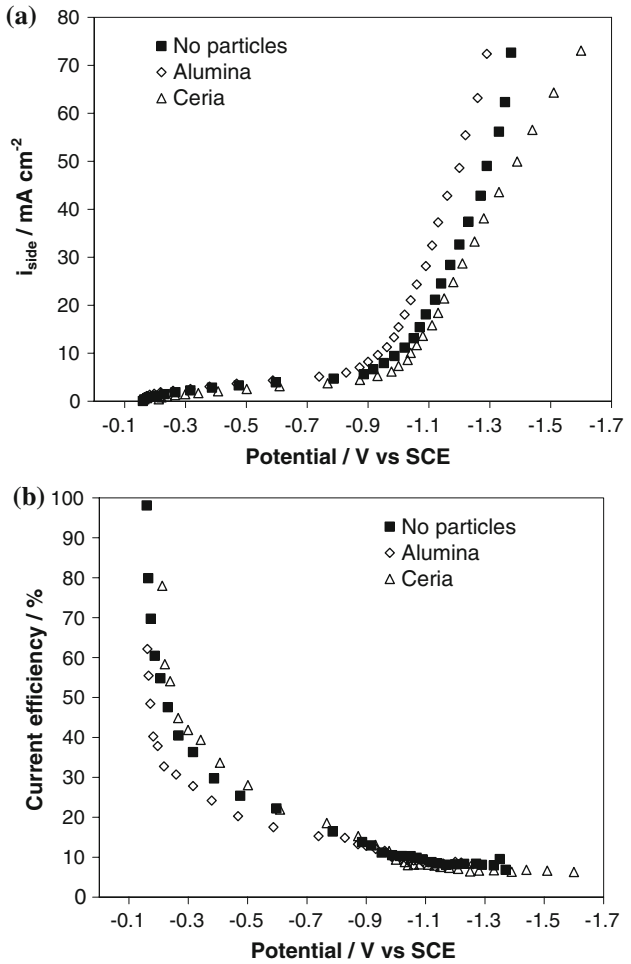

Fig. 7 Variation of (**a**) side reaction and (**b**) current efficiency with potential during the electrodeposition of NiCu alloys and NiCu-particle composites at 540 rpm

Acknowledgements This work was supported by the National Science Foundation, Grant # ECE-0202766. Dr. X. Xie is gratefully acknowledged for his help in WDS analysis.

Appendix A

The largest change of current along the RCHC is theoretically predicted by a primary current distribution approach, which assumes that field effects (i.e. ohmic conditions) control the distribution and renders it sensitive to the placement of the electrodes, cell walls and any insulating shields. Models have been developed for this particular RCHC geometry that agree well with experimental data [31]. Figure A1 shows the dimensionless distribution of current density normalized to the average applied current density along the electrode length with a primary current distribution assumption (indicated as points), provided by the manufacturer of the RCHC used here. A polynomial fit

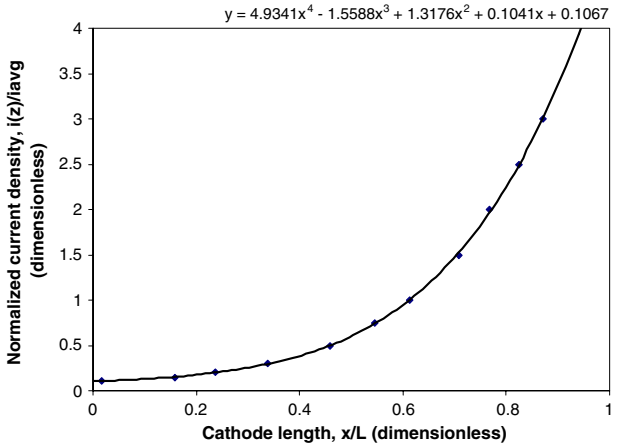

Fig. A1 Primary current distribution of the RotaHull RCHC with a fitted polynomial

to the theoretical data points (line) was used for interpolation.

References

1. Datta M, Landolt D (2000) Electrochim Acta 45:2535
2. Landolt D (1994) Electrochim Acta 39:1075
3. Fransaer J, Celis J, Roos J (1992) J Electrochem Soc 139:413
4. Ding X, Merk N, Ilschner B (1998) J Mater Sci 33:803
5. Hovestad A, Janssen L (1995) J Appl Electrochem 25:519
6. Musiani M (2000) Electrochim Acta 45:3397
7. Berkh O, Eskin S, Zahavi J (1995) Plat Surf Finish 82:72
8. Fawzy M, Ashour M, El-Halim A (1998) Trans Inst Met Finish 76:193
9. Lozano-Morales A, Fitzgerald J, Xie X, Singh V, Podlaha EJ (2006) J Electrochem Soc 153:C567
10. Panda A, Podlaha E (2003) Electrochem Solid State Lett 6:C149
11. Despa M, Kelly K, Collier J (1999) Microsyst technol-micro-nanosyst-inform storage process syst 6:60
12. Friend WZ (1980) Corrosion of Nickel and Nickel Base Alloys. Wiley, New York
13. Ghosh S, Grover A, Totlani M (1999) Bull Electrochem 15:174
14. Vu Quang K, Chassaing E, Le Viet B, Celis JP, Roos JR (1985) Met Finish 83:25
15. Ishikawa M, Enomoto H, Matsuoka M, Iwakura C (1995) Electrochim Acta 40:1663
16. Delatorre R, Sartorelli M, Schervenski A, Pasa A, Guths S (2003) J Appl Phys 93:6154
17. Bakonyi I, Toth-Kadar E, Toth J, Becsei T, Tarnoczi T, Kamasa P (1999) J Phys: Condens Matter 11:963
18. Yeo I, Johnson D (2001) J Electroanal Chem 495:110
19. Khotuleva M, Gudkov B, Slinkin A, Kiperman S (1986) Kinet Catal 27:874
20. Khulbe K, Mann R (1982) Catal Reviews-Sci Eng 24:311
21. Jayakrishnan S, Krishna N, Sujatha K, Sriveeraraghavan S, Krishnan R, Natarajan S (1996) Bull Electrochem 12:259
22. Sun S, Zhang M (1991) Acta Metallurgica Sinica (English Edition) Series B: Process Metall Miscellaneous 4:206
23. Durisin J, Durisinova K, Orolinova W, Saksl K (2005) Int J Mater Prod Technol 23:42
24. Anderson KR, Groza JR, Dreshfield RL, Ellis D (1995) Metall Mater Trans A 26A:2197

25. Lozano-Morales A, Podlaha E (2004) J Electrochem Soc 151:C478
26. Stojak J, Talbot J (2001) J Appl Electrochem 31:559
27. Zhu L, Peng X, Yan J, Wang F (2004) Oxid Met 62:411
28. Madore C, Landolt D (1993) Plat Surf Finish 80:73
29. Tannenberger H (2002) Galvanotechnik 93:938
30. Low CTJ, Ponce de Leon C, Walsh FC (2005) Aust J Chem 58:246
31. Low CTJ, Roberts EPL, Walsh FC (2007) Electrochim Acta 52:3831
32. Eisenberg M, Tobias CW, Wilke CR (1954) J Electrochem Soc 101:306
33. Hessami S, Tobias C (1989) J Electrochem Soc 136:3611